

Electronic Supporting Information

Revealing the activity and selectivity of ppm level copper in gas diffusion electrodes toward CO and CO₂ electroreduction

Xiang Lyu^{1,2}, Jianlin Li², Tianyu Zhang¹, Zhengyuan Li¹, In-hui Hwang³, Chengjun Sun³, Charles J. Jafta², Jun Yang², Todd J. Toops⁴, David A. Cullen⁵, Alexey Serov^{2*}, and Jingjie Wu^{1*}

Corresponding authors: Alexey Serov, email: serova@ornl.gov; Jingjie Wu, email: jingjie.wu@uc.edu

¹ Department of Chemical and Environmental Engineering, University of Cincinnati, Cincinnati, OH, USA

² Electrification and Energy Infrastructures Division, Oak Ridge National Laboratory; Oak Ridge, TN 37831, USA

³ X-Ray Science Division, Argonne National Laboratory, IL 60439, USA

⁴ Buildings and Transportation Science Division, Oak Ridge National Laboratory; Oak Ridge, TN 37831, USA

⁵ Center for Nanophase Materials Sciences, Oak Ridge National Laboratory, Oak Ridge, Tennessee, 37831, USA

Experimental section

Preparation of electrodes. Carbon paper (CP, Sigracet 39BB) with an area of 17.5 cm² (5 cm × 3.5 cm) was impregnated with 2 ml CuCl₂ solution of varying concentrations (solvent mixture of DI H₂O : isopropanol (IPA) = 1 : 1 v/v) for 1 h to directly load trace Cu onto the CP, as shown in Fig. S1. The solvent mixture was used instead of pure water to increase the wettability of the solvent, as the surface of the CP is highly hydrophobic. The Cu-impregnated CP was rinsed with DI water to remove the residual solution, followed by drying at 100 °C on a hot plate. Subsequently, the Cu-impregnated CP was cut into six electrodes with an area of 2.8 cm² (1.67 cm × 1.67 cm) each for repeated electrochemical measurements. The Cu content in each electrode was measured via the inductively coupled plasma optical emission spectroscopy (ICP-MS, PerkinElmer-Optima 2000DV) and is tabulated in Table S1. In this work, the CP-Cu_{0.812} electrode refers to Cu loading of 0.812 μg cm⁻² in the CP electrode. All other electrodes were named based on Cu loading. A control experiment with the CuCl₂ solution in pure DI water solvent was carried out to investigate the effect of solvent on Cu loading onto CP. One more control experiment was performed with the CP impregnated in DI H₂O and IPA mixture solvent without CuCl₂ added.

Characterization of electrodes. The Cu content in each electrode was confirmed with ICP-MS.¹ First, samples were submerged in the 500 μL concentrated nitric acid in a digestion vial. Subsequently, the vial was heated to 65 °C for a half hour (pre-digestion), followed by digestion at 130 °C for 1 h. Then 200 μL of H₂O₂ (30% v/v) was added after the vial was cooled to room temperature. The sample was further digested at 130 °C for 1 h, followed by resting at 70 °C overnight, and then heated up to 150 °C for 1 h. An additional 200 μL of H₂O₂ was added to the vial and heated to 130 °C for 10 min. The sample was diluted to 10 mL before adding internal

standards (Yttrium, High Purity Standards Inc.) prior to quantification. The ICP-MS results were normalized by the sample weight to get the final Cu content in the ng g^{-1} .

The X-ray photoelectron spectroscopy (XPS) spectra were obtained utilizing a monochromatic Al K_{α} source operating at 200 W.²⁻⁴ The pre- and post-electrodes in CORR experiments were placed on double-sided conductive carbon tape before being introduced into the ultra-high vacuum chamber. The survey and high-resolution spectra were acquired at 150 eV and 20 eV, respectively. For the high-resolution spectra of Cu, the scan rate is 0.1 eV with a scan number of 20. No charge neutralization was used during the measurements, and charge correction was applied. The calibration was based on the adventitious C 1s at the binding energy of 284.8 eV.

X-ray absorption spectroscopy (XAS) measurements of pre- and post-electrodes in CORR experiments were carried out with a fluorescence mode using a Si (111) double crystal monochromator at the 20-ID-B beamline of the Advanced Photon Sources (APS) at Argonne National Laboratory. The monochromatic X-ray beam was calibrated to the peak of the first derivative of X-ray absorption near-edge structure (XANES) at Cu K-edge from Cu foil. The XANES was extracted using Demeter, a software package for analyzing XAS, according to the standard analysis procedure.⁵

Scanning electron microscopy (SEM) was applied to characterize the microstructure of the electrodes after the CORR experiment. The images were taken in a Carl Zeiss Merlin instrument operating at 3.0 kV. Energy Dispersive X-Ray Spectroscopy (EDS) elemental mapping images were obtained for the same sample with a system from Bruker Nano GmbH using an XFlash detector 5030 at 10 kV.

Aberration-corrected scanning transmission electron microscope (AC-STEM) was employed to determine the Cu structure on CP-Cu_{0.812} electrode after CORR. High-angle annular dark field

(HAADF) and secondary electron (SE) images were recorded simultaneously using a Cs-probe corrected JEOL NEOARM electron microscope (JEOL Ltd.) operated at 80 kV with the semi-convergence angle of 6.5 mrad and probe current of ~40pA.

Contact angle (CA) measurements were carried out on the obtained electrodes with pure DI water and a mixture of DI water and IPA, and the details about the measurement can be found in previous work.⁶

Electrochemical test of the CO/CO₂RR. A homemade flow cell was applied for CO/CO₂RR experiments at ambient conditions. An anion exchange membrane (FAA-3-PK-75, Fuel Cell Store) was employed to separate anodic and cathodic compartments. Ni foam was used as the anode for oxygen evolution, and the prepared CP electrodes with different Cu loadings were applied as the cathode for CO/CO₂RR. A Hg/HgCl (saturated KCl) was used as the reference electrode. The catholyte (1M KOH) and anolyte (1M KOH) with a flow rate of 0.5 mL min⁻¹ were both controlled by a peristaltic pump (Harvard apparatus, P70-7000). The current was controlled in a galvanostatic mode, while the potential was simultaneously measured and recorded by the multi-channel function of EnergyLab XM (Solartron Analytical). The reported current density is the geometric current density unless otherwise stated. The cathode potential was measured online relative to the reference electrode. All potentials were converted to the RHE scale using Equation 1:

$$E_{RHE} = E_{Hg/HgCl} + 0.244 V + 0.0591 \times pH \quad (1)$$

An iR compensation was determined by potentiostatic electrochemical impedance spectroscopy (EIS). In CORR, the CO feedstock with a flow rate of 20 sccm was controlled by a mass flow controller (MFC, Alicat Scientific MC). The gas product stream was injected into a gas chromatograph (GC, Agilent 7890B) for quantitative analysis. In CO₂RR, the CO₂ feedstock with

the same flow rate of 20 sccm was used, while the gas product stream was mixed with 10 sccm Ar at the electrolyzer outlet before injection into the GC. Since the CO₂ flow rate in the outlet is not the same as in the inlet, the CO₂ outlet flow rate was calibrated by the Ar stream according to our previous work.⁷ The FE of each gas product was calculated based on the CO and CO₂ outlet flow rate. Meanwhile, the catholyte was collected after electrolysis in CO₂RR, followed by quantifying the liquid products via ¹H NMR (Bruker AV 400 MHz spectrometer). For each run, 500 μL of the catholyte was mixed with an internal standard of 3-(Trimethylsilyl) propionic-2,2,3,3-d₄ acid sodium salt in D₂O. The standard deviations were calculated based on the measurement of three independent experiments. Additionally, the anolyte and catholyte were collected and mixed after electrolysis in CORR, followed by the same measurement as CO₂RR, as CH₃COO⁻ was found to migrate from the cathode to anode side.

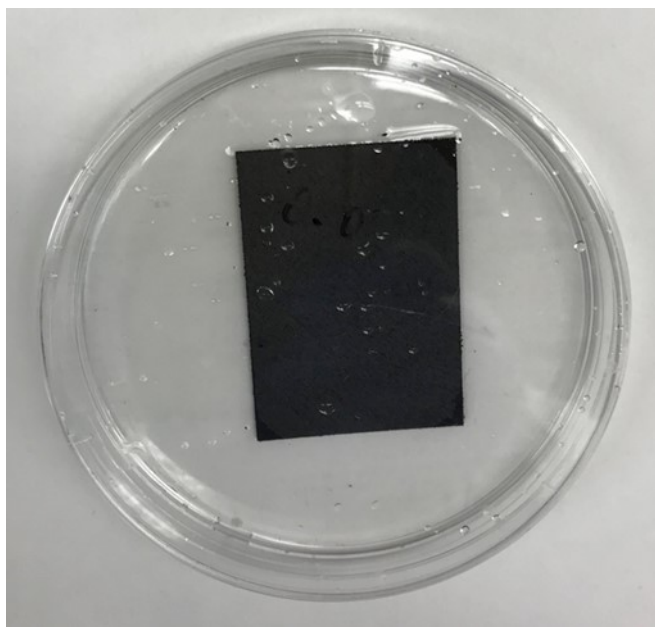


Fig. S1 Picture of loading trace Cu in CP by impregnation.

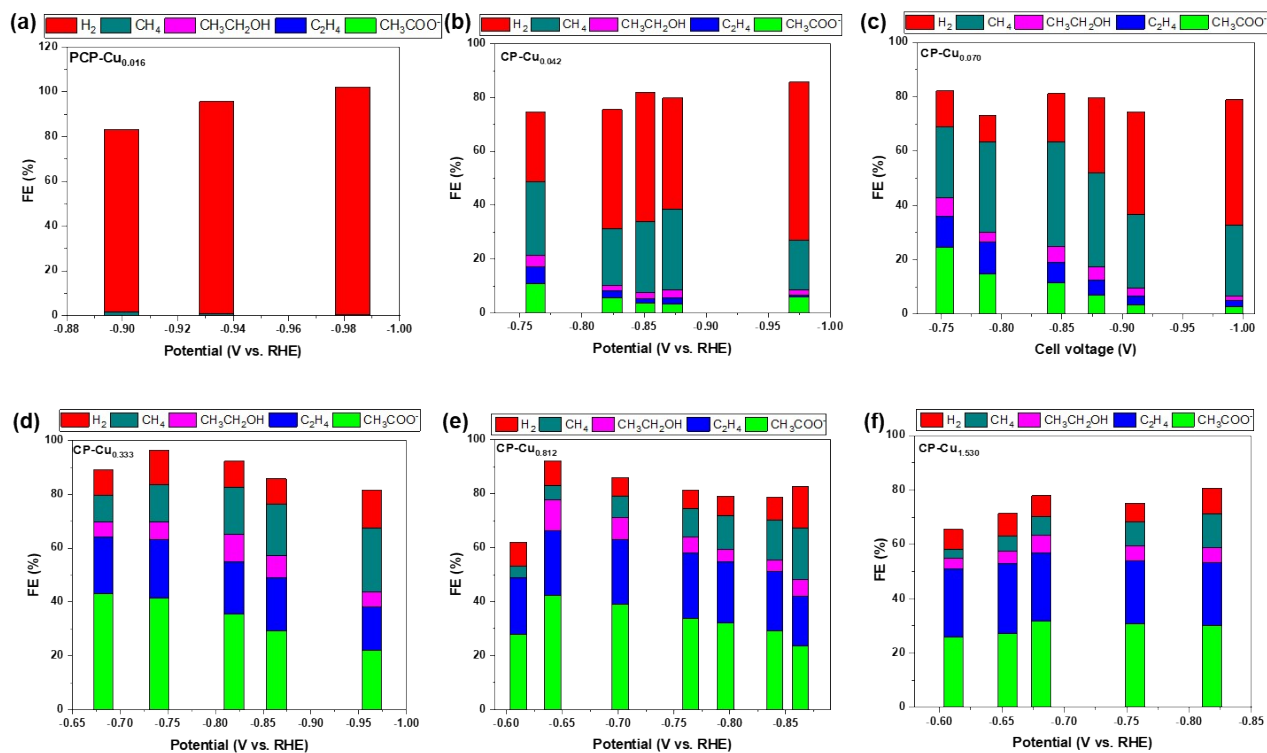


Fig. S2 FE of all products during CORR as a function of the applied potential on (a) PCP-Cu_{0.016}, (b) CP-Cu_{0.042}, (c) CP-Cu_{0.070}, (d) CP-Cu_{0.333}, (e) CP-Cu_{0.812}, and (f) CP-Cu_{1.530}.

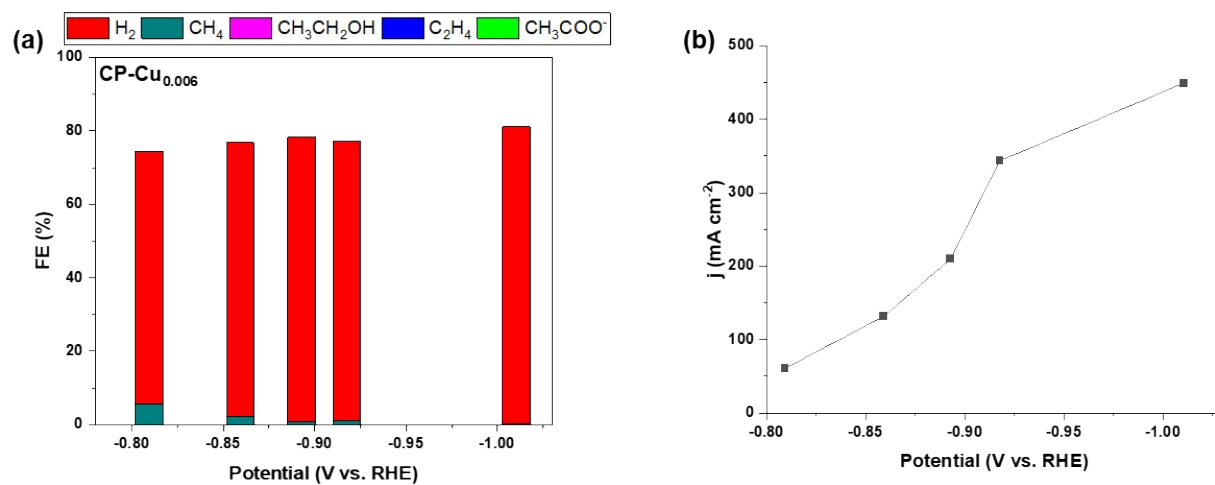


Fig. S3 (a) FE of all products during CORR using the CP impregnated in pure DI water and IPA mixture solvent without CuCl₂ for 1 h as a function of the applied potential. **(b)** The total current density.

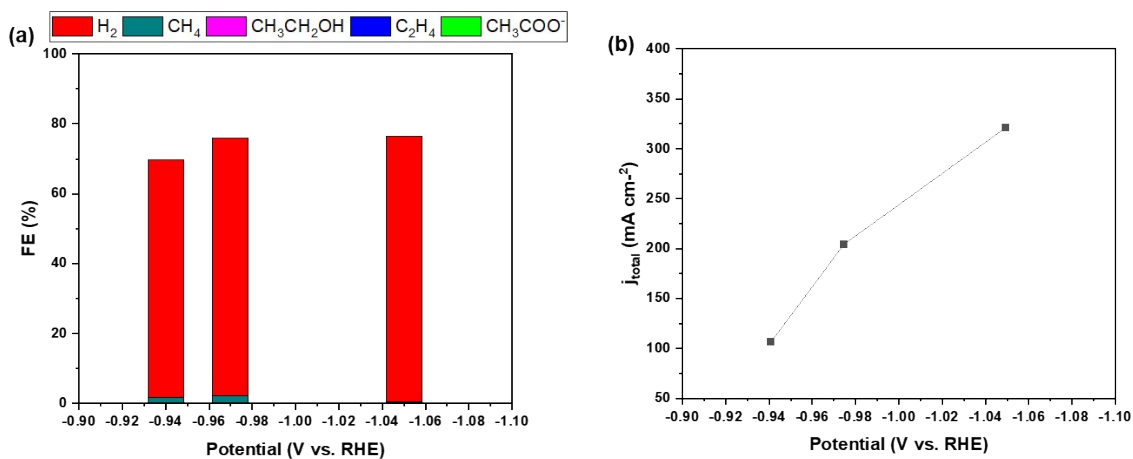


Fig. S4 (a) FE of all products during CORR using the carbon paper electrode (impregnated in 5 mM CuCl_2 with pure DI water solvent for 1 h) as a function of the applied potential. **(b)** The total current density.

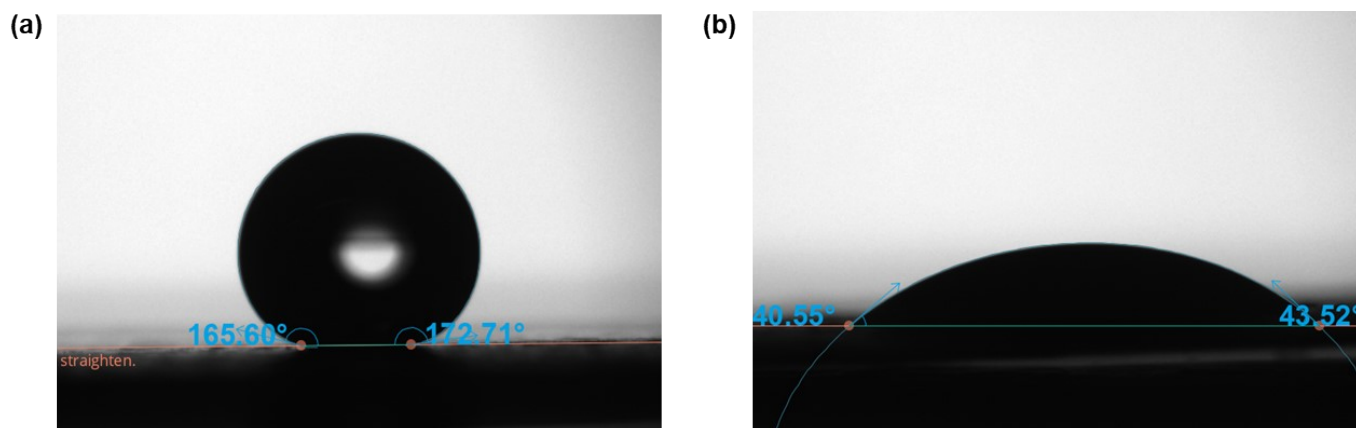


Fig. S5 Contact angle measurements on carbon paper. **(a)** 169 °C with pure DI water. **(b)** 42 °C with a mixture of DI water and IPA ($H_2O_{(v)}/IPA_{(v)}=1/1$).

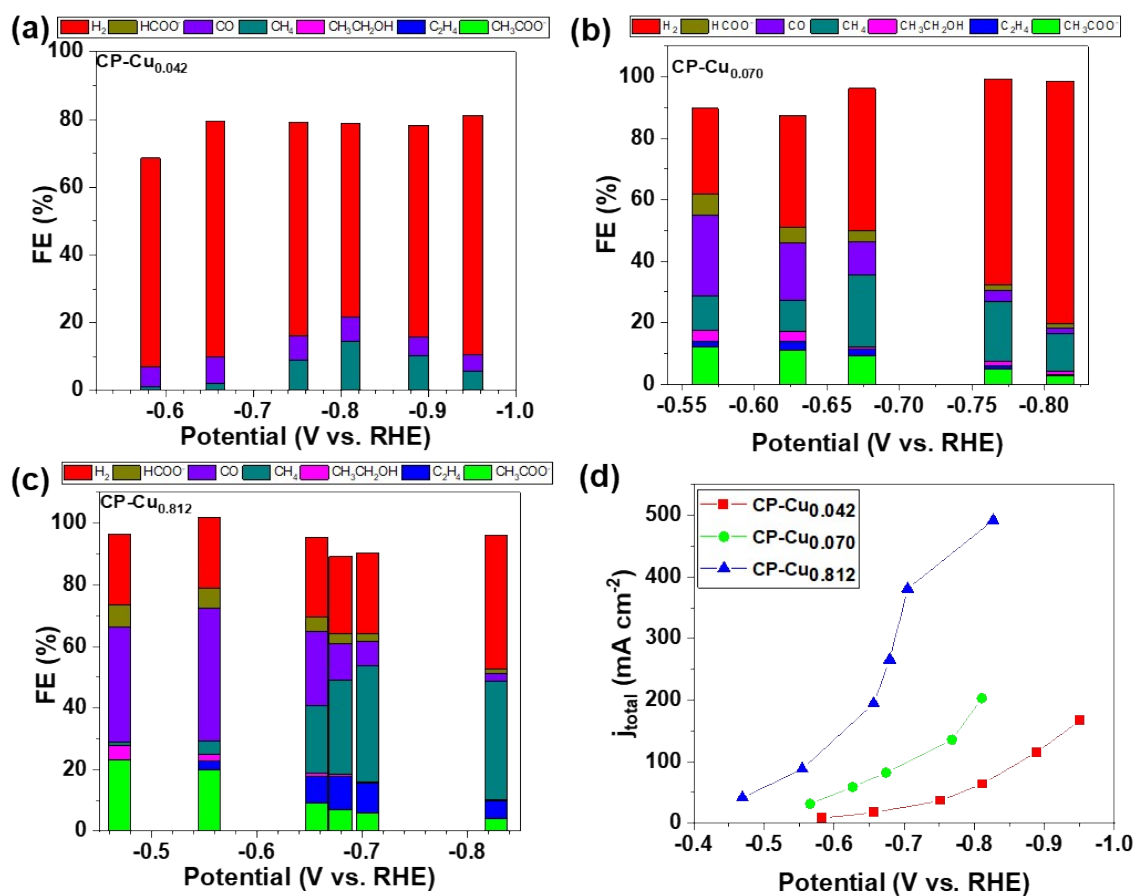


Fig. S6 FE of all products during CO₂RR as a function of the applied potential on (a) CP-Cu_{0.042}, (b) CP-Cu_{0.070}, and (c) CP-Cu_{0.812}. (d) The total current density.

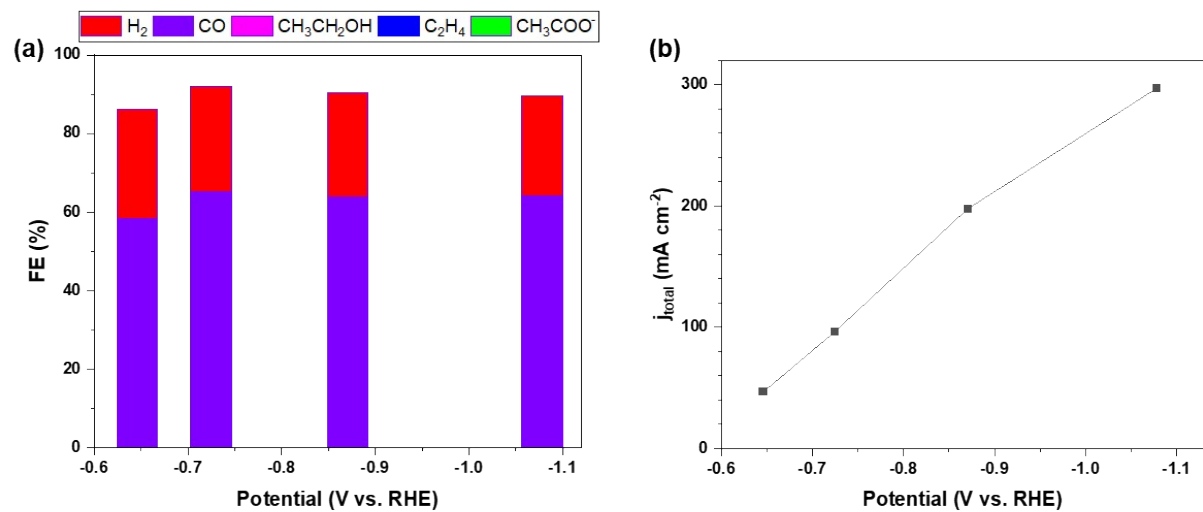


Fig. S7 (a) FE of products during CO₂RR with carbon paper being impregnated in 5 mM ZnCl₂ solution (solvent, H₂O_(v)/IPA_(v)=1/1) for 1 h. Only CO and H₂ were observed. (b) The total current density.

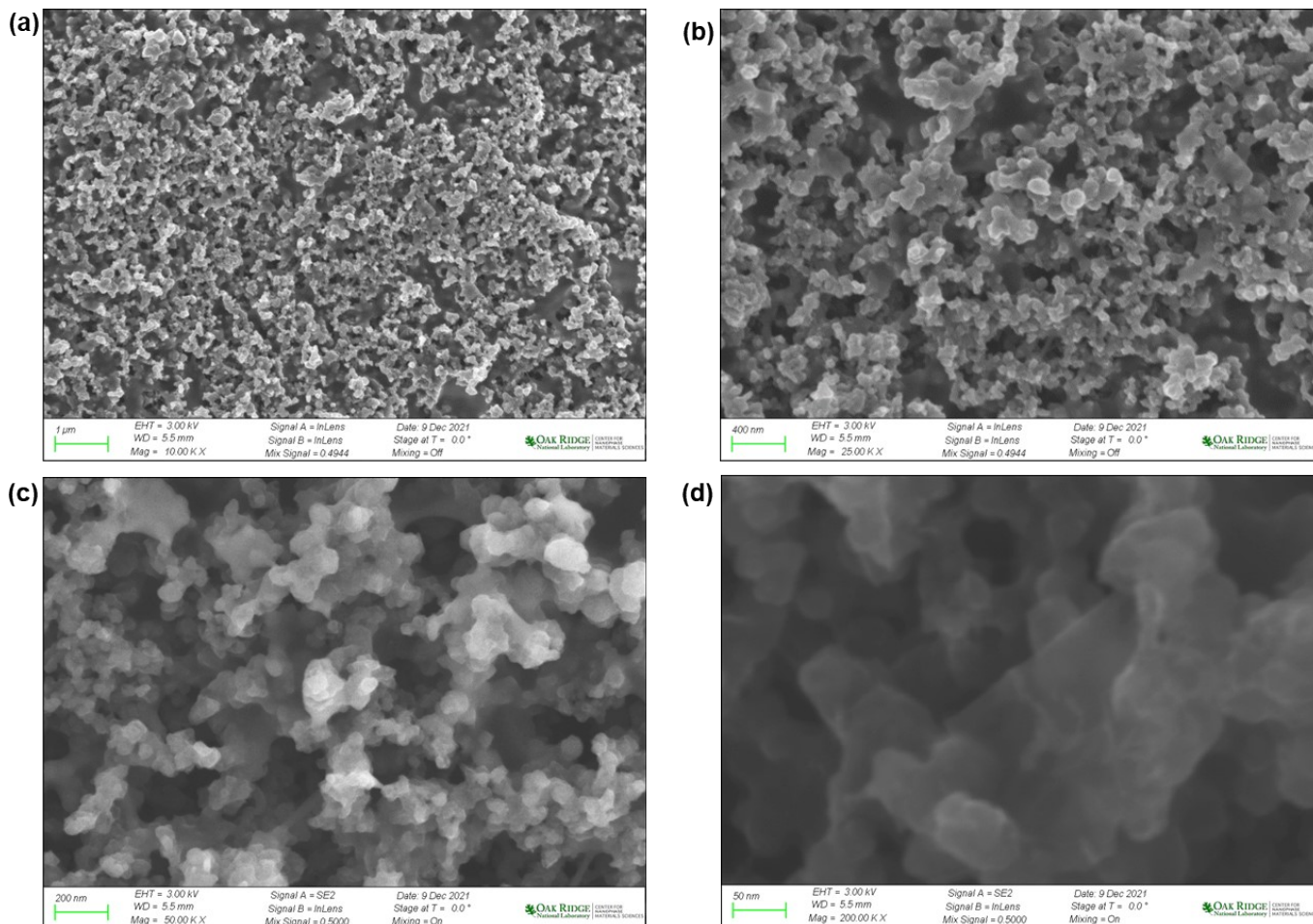


Fig. S8 SEM of CP-Cu_{0.812} electrode of (a) 10 K magnification, (b) 25 K magnification, (c) 50 K magnification, and (d) 200 K magnification.

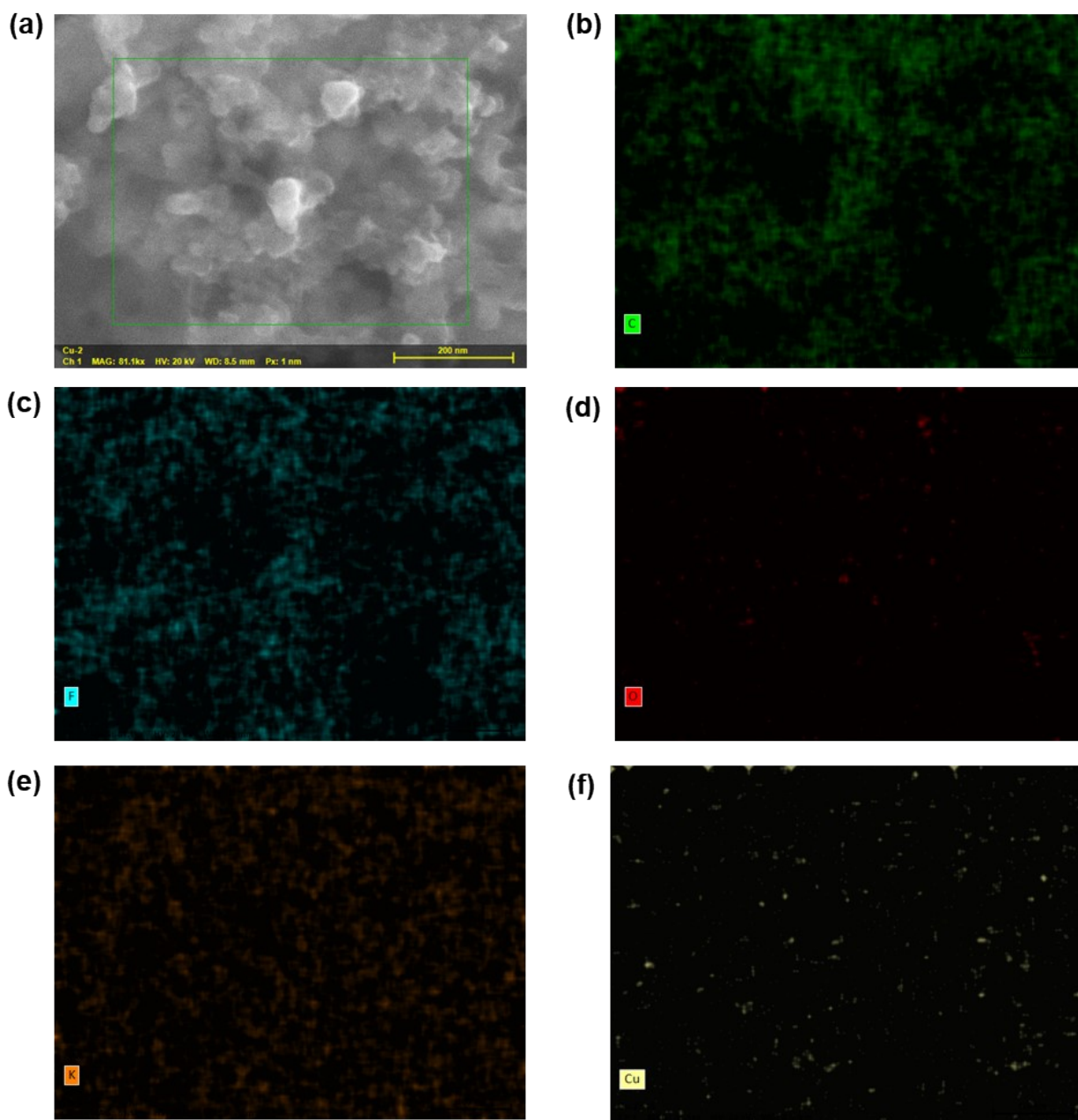


Fig. S9 EDX mapping of CP-Cu_{0.812} electrode. (a) Mapping area, mapping element of (b) C, (c) F, (d) O, (e) K, and (f) Cu.

Table S1 The loading of Cu in the carbon paper (CP) substrates prepared by impregnation in different CuCl₂ concentrations (solvent, H₂O_(v)/IPA_(v)=1/1).

CuCl ₂ (mM)	Cu content (ppm) ^a	Cu loading (μg cm ⁻²) ^b
0	0.7	0.006
0.005	4.9	0.042
0.025	8.2	0.070
0.125	38.8	0.333
0.500	94.4	0.812
5.000	177.9	1.530
Pristine CP (PCP)	1.9	0.016

^a The Cu content in electrodes was determined by ICP-MS, and all Cu content obtained included the Cu in the pristine carbon paper (1.9 ppm).

^b The loading is normalized to the geometric area of the electrode based on the Cu content from the ICP-MS measurement.

Table S2. Comparison of mass activity with different catalysts for CO/CO₂RR.

Catalysts	Potential (V vs. RHE)	Major carbon products	Mass activity (A mg ⁻¹)	Refs.
Sn-Cu alloy	-1.14 ^e	HCOO ⁻	1.49	8
Au-Fe-CSNP ^a	-0.9 ^e	CO	0.16	9
AuCeO ₂ /C	-0.6 ^e	CO	0.139	10
Cu@AuCu	-0.8 ^e	CO	0.439	11
CuN ₃ NP	-1.6 ^e	C ₂ H ₄	0.034	12
Sn _{1-x} In _x @In _{1-y} Sn _y O _z	-1.0 ^e	HCOO ⁻	0.437	13
Au/Cu NP	-0.8 ^e	CO	0.5	14
Au nanowire	-0.89 ^f	CO	0.173	15
Cu cubes	-0.75 ^f	C ₂ H ₄	0.7	16
Cu octahedra	-0.93 ^f	CH ₄	1.45	16
Fe/Au	-0.9 ^f	CO	0.399	17
Co-PPy-C	-0.7 ^e	CO	0.091	18
Cu-based NP/C	-1.16 ^e	C ₂ H ₄	0.06	19
Co Nanosheet	-0.4 ^e	CH ₃ CH ₂ OH	0.003	20
Zn/C/Ag	-0.9 ^e	CO	0.4	21
Au/pyridine/C NT ^b	-0.98 ^e	CO	0.25	22
Ag NP	-1.1 ^e	CO	0.012	23
Ag-Cu nanodimer	-1.1 ^e	C ₂ H ₄	0.03	23
Cu-N-C ^d	-1.0 ^f	C ₂ ^c	0.035	24
Cu Nanosheets ^d	-0.78 ^f	C ₂ ^c	0.36	25
Cu/GDY ^d	-1.3 ^f	CH ₄	0.04	26
Cu/GDY ^d	-1.0 ^f	C ₂ ^c	0.56	26
Cu plates ^d	-0.69 ^f	C ₂ ^c	0.67	27
Cu	-0.63 ^f	CO	155	This work
Cu	-0.77 ^f	CH ₄	375	This work
Cu ^d	-0.86 ^f	C ₂ ^c	584	This work
Cu ^d	-0.87 ^f	CH ₄	2435	This work

^a CSNP stands for core-shell nanoparticles

^b NT stands for nanotubes

^c C₂ products include CH₃COO⁻, C₂H₄, CH₃CH₂OH, and CH₃CH₂CH₂OH

^d Those experiments are for CORR, and the other experiments are for CO₂RR

^e H-type reactor

^f Flow reactor

Table S3. Comparison of turnover frequency with different catalysts for CO/CO₂RR.

Catalysts	Potential (V vs. RHE)	Major carbon products	TOF (s ⁻¹)	Refs.
Ni-C-N	-0.75 ^e	CO	0.29	28
Fe/Au	-0.9 ^f	CO	3.2	17
Trace Cu in GO ^a	-1.3 ^e	CH ₄	3.5	29
C-Zn ₁ Ni ₄	-1.13 ^e	CO	2.8	30
CoPor-N ₃	-0.6 ^e	CO	0.15	31
N ₄ -Ni-Sn-N ₄	-1.0 ^e	HCOOH	1.32	32
Ni NP	-1.0 ^e	CO	0.47	33
Tannin-Pb	-0.92 ^e	HCOOH	0.055	34
p-FeNC/NiNC	-0.9 ^e	CO	3.3	35
Ni ₅ -PTF ^b	-1.0 ^e	CO	5.6	36
Ni/NCNT ^c	-1.0 ^e	CO	2.6	37
H-NiPc/CNT	-0.94 ^e	CO	3.9	38
NiPc/NiO ₄	-1.2 ^e	CO	0.72	39
CuO NP	-1.05 ^e	C ₂ H ₄	0.05	40
Cu-N-C	-0.77 ^f	CO	0.26	41
Fe/Cu-N-C	-1.1 ^f	CO	1.4	42
Cu	-0.63 ^f	CO	51	This work
Cu	-0.7 ^f	CH ₄	31	This work
Cu ^d	-0.86 ^f	C ₂ (CH ₃ COO ⁻ , C ₂ H ₄ , and CH ₃ CH ₂ OH)	145	This work
Cu ^d	-0.87 ^f	CH ₄	267	This work

^a GO stands for graphene oxide

^b PTF stands for porpyhrinic triazine framework

^c NCNT stands for N-doped carbon nanotube

^d Those two experiments are for CORR, and the other experiments are for CO₂RR

^e H-type reactor

^f Flow reactor

Supplementary references

1. T. Zhang, W. Li, K. Huang, H. Guo, Z. Li, Y. Fang, R. M. Yadav, V. Shanov, P. M. Ajayan and L. Wang, *Nature communications*, 2021, **12**, 1-9.
2. T. Reshетенko, M. Odgaard, G. Randolph, K. K. Ohtaki, J. P. Bradley, B. Zulevi, X. Lyu, D. A. Cullen, C. J. Jafta, A. Serov and A. Kulikovskiy, *Applied Catalysis B: Environmental*, 2022, **312**, 121424.
3. A. Sveinbjörnsson, A. B. Gunnarsdóttir, E. B. Creel, C. P. Canales, B. Zulevi, X. Lyu, C. J. Jafta, E. Skúlason, A. Serov and H. D. Flosadóttir, *SusMat*, 2022.
4. X. Lyu, J. Li, C. J. Jafta, Y. Bai, C. P. Canales, F. Magnus, Á. S. Ingason and A. Serov, *Journal of Environmental Chemical Engineering*, 2022, **10**, 108486.
5. B. Ravel and M. Newville, *Journal of synchrotron radiation*, 2005, **12**, 537-541.
6. J. Sharma, G. Polizos, C. J. Jafta, Y. Bai, D. Hun and X. Lyu, *RSC Advances*, 2022, **12**, 15373-15377.
7. T. Y. Zhang, Z. Y. Li, J. F. Zhang and J. J. Wu, *Journal of Catalysis*, 2020, **387**, 163-169.
8. K. Ye, A. Cao, J. Shao, G. Wang, R. Si, N. Ta, J. Xiao and G. Wang, *Science Bulletin*, 2020, **65**, 711-719.
9. K. Sun, T. Cheng, L. Wu, Y. Hu, J. Zhou, A. MacLennan, Z. Jiang, Y. Gao, W. A. Goddard III and Z. Wang, *Journal of the American Chemical Society*, 2017, **139**, 15608-15611.
10. J. Fu, D. Ren, M. Xiao, K. Wang, Y. Deng, D. Luo, J. Zhu, G. Wen, Y. Zheng and Z. Bai, *ChemSusChem*, 2020, **13**, 6621-6628.
11. S. Dai, T.-H. Huang, W.-I. Liu, C.-W. Hsu, S.-W. Lee, T.-Y. Chen, Y.-C. Wang, J.-H. Wang and K.-W. Wang, *Nano Letters*, 2021, **21**, 9293-9300.
12. Z. Yin, C. Yu, Z. Zhao, X. Guo, M. Shen, N. Li, M. Muzzio, J. Li, H. Liu and H. Lin, *Nano letters*, 2019, **19**, 8658-8663.
13. L. C. Pardo Pérez, D. Teschner, E. Willinger, A. Guier, M. Driess, P. Strasser and A. Fischer, *Advanced Functional Materials*, 2021, **31**, 2103601.
14. D. R. Kauffman, D. R. Alfonso, D. N. Tafen, C. Wang, Y. Zhou, Y. Yu, J. W. Lekse, X. Deng, V. Espinoza and J. Trindell, *The Journal of Physical Chemistry C*, 2018, **122**, 27991-28000.
15. M. Cho, J. M. Kim, B. Kim, S. Yim, Y. J. Kim, Y. S. Jung and J. Oh, *Journal of Materials Chemistry A*, 2019, **7**, 6045-6052.
16. G. L. De Gregorio, T. Burdyny, A. Loiudice, P. Iyengar, W. A. Smith and R. Buonsanti, *ACS catalysis*, 2020, **10**, 4854-4862.
17. X. Shen, X. Liu, S. Wang, T. Chen, W. Zhang, L. Cao, T. Ding, Y. Lin, D. Liu and L. Wang, *Nano Letters*, 2020, **21**, 686-692.
18. Y. Mun, K. Kim, S. Kim, S. Lee, S. Lee, S. Kim, W. Choi, S.-k. Kim, J. W. Han and J. Lee, *Applied Catalysis B: Environmental*, 2018, **236**, 154-161.
19. H. Jung, S. Y. Lee, C. W. Lee, M. K. Cho, D. H. Won, C. Kim, H.-S. Oh, B. K. Min and Y. J. Hwang, *Journal of the American Chemical Society*, 2019, **141**, 4624-4633.
20. J. Yin, Z. Yin, J. Jin, M. Sun, B. Huang, H. Lin, Z. Ma, M. Muzzio, M. Shen and C. Yu, *Journal of the American Chemical Society*, 2021, **143**, 15335-15343.
21. Y. Gao, F. Li, P. Zhou, Z. Wang, Z. Zheng, P. Wang, Y. Liu, Y. Dai, M.-H. Whangbo and B. Huang, *Journal of Materials Chemistry A*, 2019, **7**, 16685-16689.
22. Z. Ma, C. Lian, D. Niu, L. Shi, S. Hu, X. Zhang and H. Liu, *ChemSusChem*, 2019, **12**, 1724-1731.

23. J. Huang, M. Mensi, E. Oveisi, V. Mantella and R. Buonsanti, *Journal of the American Chemical Society*, 2019, **141**, 2490-2499.
24. X. Fu, Y. Wang, H. Shen, Y. Yu, F. Xu, G. Zhou, W. Xie, R. Qin, C. Dun and C.-W. Pao, *Materials Today Physics*, 2021, **19**, 100418.
25. W. Luc, X. Fu, J. Shi, J.-J. Lv, M. Jouny, B. H. Ko, Y. Xu, Q. Tu, X. Hu and J. Wu, *Nature Catalysis*, 2019, **2**, 423-430.
26. X. K. Li, L. H. Jiang, J. Liu, Q. F. Hua, E. D. Wang and G. W. Xie, *J. Energy Chem.*, 2020, **43**, 121-128.
27. R. Xia, J.-J. Lv, X. Ma and F. Jiao, *Journal of Catalysis*, 2021, **398**, 185-191.
28. F. Pan, W. Deng, C. Justiniano and Y. Li, *Applied Catalysis B: Environmental*, 2018, **226**, 463-472.
29. Y. Lum, Y. Kwon, P. Lobaccaro, L. Chen, E. L. Clark, A. T. Bell and J. W. Ager, *Acs Catalysis*, 2016, **6**, 202-209.
30. C. Yan, H. Li, Y. Ye, H. Wu, F. Cai, R. Si, J. Xiao, S. Miao, S. Xie and F. Yang, *Energy & Environmental Science*, 2018, **11**, 1204-1210.
31. T. Wang, L. Guo, H. Pei, S. Chen, R. Li, J. Zhang and T. Peng, *Small*, 2021, **17**, 2102957.
32. S. G. Han, D. D. Ma and Q. L. Zhu, *Small Methods*, 2021, **5**, 2100102.
33. Z. Li, D. He, X. Yan, S. Dai, S. Younan, Z. Ke, X. Pan, X. Xiao, H. Wu and J. Gu, *Angewandte Chemie*, 2020, **132**, 18731-18736.
34. Y. Shi, Y. Ji, J. Long, Y. Liang, Y. Liu, Y. Yu, J. Xiao and B. Zhang, *Nature communications*, 2020, **11**, 1-10.
35. X. Yang, M. Wang, M. J. Zachman, H. Zhou, Y. He, S. Liu, H.-Y. Zang, Z. Feng and G. Wu, *Small Science*, 2021, **1**, 2100046.
36. Q. Wu, J. Liang, Z.-L. Xie, Y.-B. Huang and R. Cao, *ACS Materials Letters*, 2021, **3**, 454-461.
37. Y. Hou, Y.-L. Liang, P.-C. Shi, Y.-B. Huang and R. Cao, *Applied Catalysis B: Environmental*, 2020, **271**, 118929.
38. Y. J. Sa, H. Jung, D. Shin, H. Y. Jeong, S. Ringe, H. Kim, Y. J. Hwang and S. H. Joo, *ACS Catalysis*, 2020, **10**, 10920-10931.
39. J. D. Yi, D. H. Si, R. Xie, Q. Yin, M. D. Zhang, Q. Wu, G. L. Chai, Y. B. Huang and R. Cao, *Angewandte Chemie*, 2021, **133**, 17245-17251.
40. S. Y. Lee, S. Y. Chae, H. Jung, C. W. Lee, D. L. T. Nguyen, H.-S. Oh, B. K. Min and Y. J. Hwang, *Journal of Materials Chemistry A*, 2020, **8**, 6210-6218.
41. S. Chen, Y. Li, Z. Bu, F. Yang, J. Luo, Q. An, Z. Zeng, J. Wang and S. Deng, *Journal of Materials Chemistry A*, 2021, **9**, 1705-1712.
42. M. Feng, X. Wu, H. Cheng, Z. Fan, X. Li, F. Cui, S. Fan, Y. Dai, G. Lei and G. He, *Journal of Materials Chemistry A*, 2021, **9**, 23817-23827.